

AD-A167 424

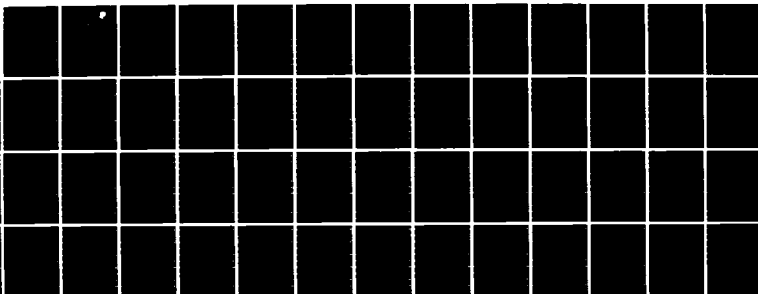
ANALYSIS OF HIGH POWER RF WINDOWS FOR GYROTRONS(U) UTAH 1/1
UNIV SALT LAKE CITY DEPT OF ELECTRICAL ENGINEERING
A G KRYCUK JAN 86 UTEC-85-000 RADC-TR-85-254

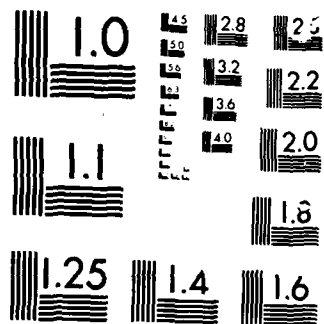
UNCLASSIFIED

F30602-82-C-0161

F/G 9/5

NL





MICROCOPY

CHART

12

AD-A167 424

RADC-TR-85-254
Final Technical Report
January 1986



ANALYSIS OF HIGH POWER RF WINDOWS FOR GYROTRONS

University of Utah

Anton George Krycuk

APPROVED FOR PUBLIC RELEASE; DISTRIBUTION UNLIMITED



ROME AIR DEVELOPMENT CENTER
Air Force Systems Command
Griffiss Air Force Base, NY 13441-5700

DTIC FILE COPY

86 5 5 030

This report has been reviewed by the RADC Public Affairs Office (PA) and is releasable to the National Technical Information Service (NTIS). At NTIS it will be releasable to the general public, including foreign nations.

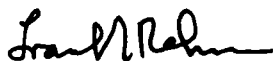
RADC-TR-85-254 has been reviewed and is approved for publication.

APPROVED:



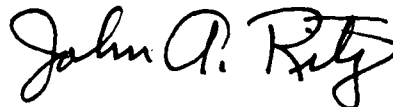
ANDREW E. CHROSTOWSKI, 1LT, USAF
Project Engineer

APPROVED:



FRANK J. REHM
Technical Director
Surveillance Division

FOR THE COMMANDER:



JOHN A. RITZ
Plans & Programs Division

If your address has changed or if you wish to be removed from the RADC mailing list, or if the addressee is no longer employed by your organization, please notify RADC (OCTP) Griffiss AFB NY 13441-5700.

Do not return copies of this report unless contractual obligations or notices on a specific document requires that it be returned.

UNCLASSIFIED

SECURITY CLASSIFICATION OF THIS PAGE

AD-A167424

REPORT DOCUMENTATION PAGE

1a REPORT SECURITY CLASSIFICATION UNCLASSIFIED			1b RESTRICTIVE MARKINGS N/A		
2a SECURITY CLASSIFICATION AUTHORITY N/A			3 DISTRIBUTION/AVAILABILITY OF REPORT Approved for public release; distribution unlimited.		
2b DECLASSIFICATION/DOWNGRADING SCHEDULE N/A					
4 PERFORMING ORGANIZATION REPORT NUMBER(S) UTEC 85-080			5 MONITORING ORGANIZATION REPORT NUMBER(S) RADC-TR-85-254		
6a NAME OF PERFORMING ORGANIZATION University of Utah		6b OFFICE SYMBOL (if applicable)	7a NAME OF MONITORING ORGANIZATION Rome Air Development Center (OCTP)		
6c ADDRESS (City, State, and ZIP Code) Department of Electrical Engineering Salt Lake City UT 84112			7b ADDRESS (City, State, and ZIP Code) Griffiss AFB NY 13441-5700		
8a NAME OF FUNDING/SPONSORING ORGANIZATION AFOSR		8b OFFICE SYMBOL (if applicable) NE	9 PROCUREMENT INSTRUMENT IDENTIFICATION NUMBER F30602-82-C-0161		
8c ADDRESS (City, State, and ZIP Code) Bolling AFB Wash DC 20332			10 SOURCE OF FUNDING NUMBERS		
			PROGRAM ELEMENT NO 61102F	PROJECT NO 2305	TASK NO J9
			WORK UNIT ACCESSION NO 16		
11 TITLE (Include Security Classification) ANALYSIS OF HIGH POWER RF WINDOWS FOR GYROTRONS					
12 PERSONAL AUTHOR(S) Anton George Krycuk					
13a TYPE OF REPORT Final		13b TIME COVERED FROM Sep 82 TO Sep 85		14 DATE OF REPORT (Year, Month, Day) January 1986	
15 PAGE COUNT 60					
16 SUPPLEMENTARY NOTATION Research accomplished in conjunction with Air Force Thermionics Engineering Research Program (AFTER)					
17 COSATI CODES			18 SUBJECT TERMS (Continue on reverse if necessary and identify by block number)		
FIELD 09	GROUP 03	SUB-GROUP	Gyrotrons Numerical Optimization High Power RF Windows		
19 ABSTRACT (Continue on reverse if necessary and identify by block number)					
<p>The project described in this report was undertaken with a view toward simplifying the multidisk dielectric window design process for gyrotrons. In the past, this procedure was involved in analyzing the response of many discrete combinations of window thicknesses in an effort to locate the optimum configurations. This report presents a method of numerically optimizing the design procedure.</p> <p>To begin with, it must be remembered that the window region of the gyrotron is severely overmoded, so care must be taken that the window must be able to pass the energy contained in the high power modes so as to avoid overheating or reflection. To this end, the first part of this paper deals with a numerical solution of Solimar's modified telegraphist equation, which allows for the mode content intercepting upon the window to be found.</p> <p>The actual window design optimization is accomplished through the use of an n dimensional</p>					
20 DISTRIBUTION/AVAILABILITY OF ABSTRACT <input checked="" type="checkbox"/> UNCLASSIFIED/UNLIMITED <input type="checkbox"/> SAME AS RPT <input type="checkbox"/> DTIC USERS			21 ABSTRACT SECURITY CLASSIFICATION UNCLASSIFIED		
22a NAME OF RESPONSIBLE INDIVIDUAL Andrew E. Chrostowski, 1/Lt., USAF			22b TELEPHONE (Include Area Code) (315) 330-4381		22c OFFICE SYMBOL RADC (OCTP)

DD FORM 1473, 84 MAR

83 APR edition may be used until exhausted
All other editions are obsoleteSECURITY CLASSIFICATION OF THIS PAGE
UNCLASSIFIED

UNCLASSIFIED

simplex method, where n is the number of window elements. Criteria delineating the search region are presented as well as typical problems which could be encountered during the optimization process.

Results are given for both the mode content and the optimization. Mode content was compared against results given by a comparable proven algorithm, while window parameters were checked against existing designs. As will be seen, correlation in both cases was very good.

UNCLASSIFIED

ACKNOWLEDGEMENTS

This thesis work was pursued under the joint sponsorship of the United States Air Force and the Electron Dynamics Division of Hughes Aircraft Company in conjunction with the University of Utah under the Air Force Thermionic Engineering and Research Program.

Additionally, this paper would not have been possible without the support and contributions of the following people: at the University of Utah, Drs. R. Grow and J. Mark Baird, who provided invaluable theoretical and moral aid, and at Hughes Aircraft Company, R. L. Woods, J. Christenson, and J. Tancredi, who allowed the theoretical to be put into practice. And, of course, my parents.

Accession No.	
NTIS	<input checked="" type="checkbox"/>
DTIC	<input type="checkbox"/>
Unannounced	<input type="checkbox"/>
Justification	
By _____	
Distribution/	
Availability Codes	
Dist	Special
A-1	



TABLE OF CONTENTS

<u>Section</u>		<u>Page</u>
I.	INTRODUCTION	1
II.	THEORETICAL FORMULATION	3
III.	NUMERICAL FORMULATION AND OPTIMIZATION	20
IV.	CALCULATED RESULTS	36
V.	CONCLUSIONS	46

LIST OF ILLUSTRATIONS

<u>Figure</u>		<u>Page</u>
1	917H gyrotron layout.	4
2	Coupling coefficients.	6
3	Waveguide geometry.	8
4	Mode conversion.	13
5	Window geometry.	15
6	Two port network.	17
7	Riccatti transforms of Solymer's equations.	25
8	Two dimensional simplex.	30
9	Global and local minima.	32
10	Mode content.	37
11	28 GHz window parameters.	38
12	28 GHz window response.	39
13	60 GHz window parameters.	40
14	60 GHz window response.	41
15	100 GHz window parameters.	42
16	100 GHz window response.	43

I. INTRODUCTION

In recent years there has been a great interest in the development of sources of high power millimeter waves for both electron cyclotron resonance heating of fusion plasmas and millimeter radar. Perhaps the most promising of these sources is the gyrotron, where the rotational energy of a spinning electron beam is coupled into a RF wave. The relative simplicity of fabrication and high theoretical efficiency (>50 percent) have made gyrotrons particularly attractive for these applications.

However, regardless of these advantages the gyrotron is nonetheless a vacuum tube device and as such requires an output coupling window in order to allow extraction of energy while maintaining vacuum integrity. Should this window present a poor match, a significant portion of the output power of the tube will, through reflection and/or loss, be prevented from being transmitted, decreasing the actual efficiency of the tube.

Current methods of window design involve the use of lumped circuit element equivalents to model the window region. These techniques assume that the region in which the window is located is cutoff to all but one (or at most very few) modes. The physical dimensions of the window are then determined pursuant to the desired RF characteristics.

These methods are not overly accurate when applied to windows to be used in gyrotrons. Unlike most other microwave tubes, a gyrotron produces

a high frequency, high power RF signal propagating in a highly overmoded waveguide. Therefore, a technique for designing gyrotron windows is required.

This report presents one way in which such a design could be accomplished. It is based on methods developed in the field of laser optics, a regime noted for severely overmoded high power systems. In addition, this paper contains a routine which allows for the estimation of the mode content of the energy intercepting upon the window.

II. THEORETICAL FORMULATION

A. MODE CONVERSION IN TAPERED WAVEGUIDES

In order to accurately design a window for maximum efficiency, it is necessary to ensure that the window is able to transmit all of the modes impinging upon it. Whereas a gyrotron cavity is designed to couple energy into one selected mode, the remainder of the tube geometry is under no such constraint. As can be seen in Figure 1, there is an uptaper from the cavity into the collector, and a further downtaper from the collector to the window.

The net effect of these tapers is to allow energy to couple out of the main mode into undesired spurious modes. Due to the increased diameter of the tube at this point, these spurious modes are not cutoff. Such a region can in fact allow a large number of modes to exist. As an example, at 60 GHz a region 2 inches in diameter would permit 263 modes to propagate.

The magnitude of the mode conversion can be computed by the use of the generalized telegraphist's equations:

$$-\frac{dV_i}{dz} = j \epsilon_i K_i I_i - \sum_p T_{pi} V_p \quad (1)$$

$$-\frac{dI_i}{dz} = j \frac{\epsilon_i}{K_i} V_i + \sum_p T_{ip} I_p \quad (2)$$

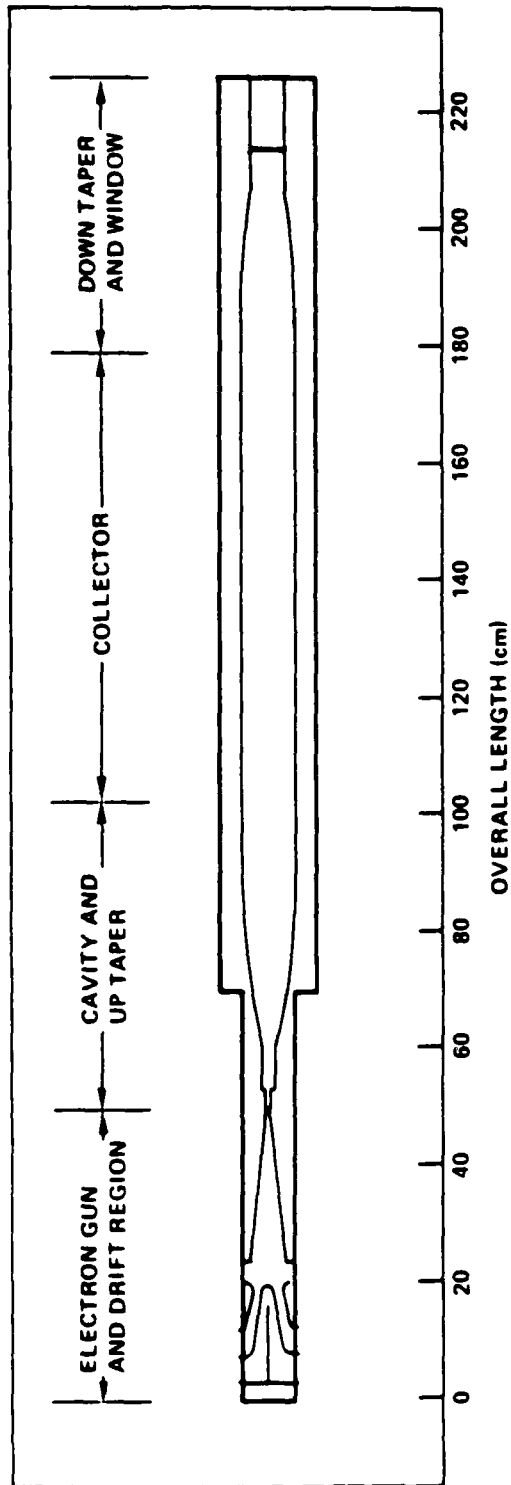


Figure 1 917H gyrotron layout.

The subscripts i and p indicate various modes. Solymar¹ has defined the amplitude of the forward and backward waves (A_i^+ and A_i^-) as

$$V_i = K_i^{1/2} (A_i^+ + A_i^-) \quad (3)$$

$$I_i = K_i^{-1/2} (A_i^- + A_i^+) \quad (4)$$

Rewriting (1) and (2) in terms of A_i^+ and A_i^- , one obtains

$$\frac{dA_i^+(z)}{dz} = -j \varepsilon_i A_i^+ - \frac{1}{2} \frac{d(\ln K_i)}{dz} A_i^- + \sum_p (S_{ip}^+ A_p^+ + S_{ip}^- A_p^-) \quad (5)$$

$$\frac{dA_i^-(z)}{dz} = +j \varepsilon_i A_i^- - \frac{1}{2} \frac{d(\ln K_i)}{dz} A_i^+ + \sum_p (S_{ip}^- A_p^+ + S_{ip}^+ A_p^-) \quad (6)$$

The coupling coefficient from the p^{th} to the i^{th} mode S_{ip}^{\pm} (+ indicates forward coupling, - backward) may be defined in terms of the transfer function T_{pi} of (1, 2) as

$$S_{ip}^{\pm} = \frac{1}{2} \left[\left(\frac{K_p}{K_i} \right)^{1/2} T_{pi} \mp \left(\frac{K_i}{K_p} \right)^{1/2} T_{ip} \right] \quad (7)$$

Solymar has provided a table of the various values of the coupling coefficient. The portion of the table of interest to this paper is reproduced in Figure 2.

$$1) \quad TM_i - TM_i \quad S_{ii}^- = -\frac{1}{2} \oint_c \tan \theta \psi_i \left(\frac{\partial \psi_i}{\partial n} \right)^2 ds$$

$$2) \quad TE_i - TE_i \quad S_{ii}^- = -\frac{1}{2} \oint_c \tan \theta \psi_i \left(\frac{\partial \psi_i}{\partial n} \right)^2 ds$$

$$3) \quad S_{ii}^+ = 0$$

$$4) \quad TM_i - TM_p \quad S_{ip}^\pm = \frac{\beta_i h_p^2 \pm \beta_p h_i^2}{2 \sqrt{\beta_i \beta_p} (h_i^2 - h_p^2)} \oint_c \tan \theta \frac{\partial \psi_i}{\partial n} \frac{\partial \psi_p}{\partial n} ds$$

$$5) \quad TM_i - TM_p \quad S_{ip}^\pm = \frac{k}{2 \sqrt{\beta_i \beta_p}} \oint_c \tan \theta \frac{\partial \psi_i}{\partial n} \frac{\partial \psi_p}{\partial n} ds$$

$$6) \quad TE_i - TE_p \quad S_{ip}^\pm = \frac{1}{2 \sqrt{\beta_i \beta_p} (h_i^2 - h_p^2)} \left[\beta_i h_p^2 \oint_c \tan \theta \psi_p \frac{\partial^2 \psi_i}{\partial n^2} ds \right. \\ \left. \pm \beta_p h_i^2 \oint_c \tan \theta \psi_i \frac{\partial^2 \psi_p}{\partial n^2} ds \right]$$

Figure 2 Coupling coefficients.

The majority of gyrotrons in production today operate in a TE mode, so equations (5) and (6) of Figure 2 need to be examined with greater scrutiny. First, define the axisymmetric elementary wave function (the solution to the Helmholtz equation in a cylindrical axisymmetric conductor) for TE modes as

$$\psi = J_n \left(\frac{P_{ni}\rho}{a} \right) \cos n \phi e^{-jk_z z} \quad (8)$$

where P_{ni} is the i^{th} root of $J'_n(x) = 0$. However, in order to determine $S_{[i][p]}^{\pm}$, it is not ψ itself that is of interest, but rather $\partial^2 \psi / \partial n^2$. As can be seen from Figure 3, the normal vector \hat{n} is identical to $\hat{\rho}$ for a cylindrical waveguide. Therefore, one finds that

$$\frac{\partial \psi}{\partial n} = \frac{\partial \psi}{\partial \rho} = \cos n \phi e^{-jk_z z} \frac{\partial}{\partial \rho} J_n \left(\frac{P_{ni}\rho}{a} \right) \quad (9)$$

Applying the Bessel function derivative relationship

$$J'_n(x) = \frac{n}{x} J_n(x) - J_{n+1}(x)$$

one obtains

$$\frac{\partial \psi}{\partial \rho} = \left[\frac{na}{P_{ni}\rho} J_n \left(\frac{P_{ni}\rho}{a} \right) - J_{n+1} \left(\frac{P_{ni}\rho}{a} \right) \right] \cos n \phi e^{-jk_z z} \quad (10)$$

Differentiating again with respect to ρ yields

$$\frac{\partial^2 \psi}{\partial \rho^2} = \left[\left(\frac{na}{P_{ni}\rho} \right)^2 - \frac{na}{P_{ni}\rho^2} - 1 \right] J_n \left(\frac{P_{ni}\rho}{a} \right) \cos n \phi e^{-jk_z z} \quad (11)$$

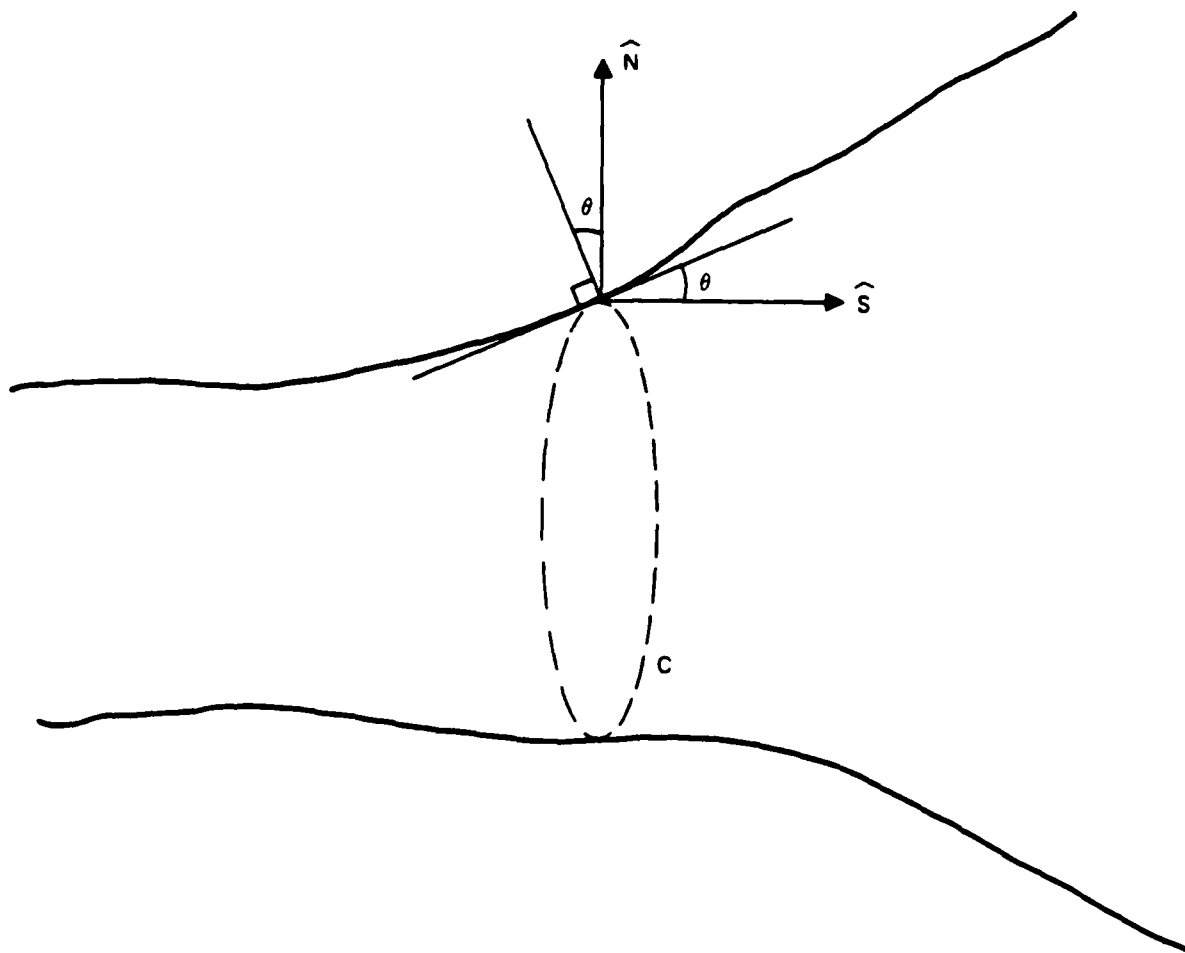


Figure 3 Waveguide geometry.

Let us now define the above mode to be ψ_{ni} rather than ψ , and furthermore let there exist some other wave function ψ_{mj} such that

$$\psi_{mj} = J_m \left(\frac{P_{mj} \rho}{a} \right) \cos m \phi e^{-jk_z z} \quad (12)$$

Upon examination of the formula for the coupling coefficient, it can be seen that the critical terms consist of two similar line integrals around the waveguide. Due to this similarity, it will be necessary to examine only one of these integrals, allowing the complimentary solution to be written from duality.

The integral to be evaluated is

$$\begin{aligned} I &= \oint_c \tan \theta \psi_{mj} \frac{\partial^2 \psi_{ni}}{\partial \rho^2} ds = \oint_c \tan \theta \psi_{mj} \frac{\partial^2 \psi_{ni}}{\partial \rho^2} \rho d\phi \\ &= \int_0^{2\pi} \tan \theta \rho J_m \left(\frac{P_{mj} \rho}{a} \right) \bigg|_{\rho=a} \left[\left(\frac{na}{P_{ni} \rho} \right)^2 - \left(\frac{na}{P_{ni} \rho^2} \right) - 1 \right] \bigg|_{\rho=a} \\ &\quad J_n \left(\frac{P_{ni} \rho}{a} \right) \bigg|_{\rho=a} \cos m \phi \cos n \phi d\phi \end{aligned} \quad (13)$$

This equation can be simplified to

$$I = f(\rho) \int_0^{2\pi} \cos m \phi \cos n \phi d\phi \quad (14)$$

which is easily solved through application of the well known orthogonality condition for trigonometric functions

$$\int_0^\pi \cos m \phi \cos n \phi d\phi = \begin{cases} 0 & m \neq n \\ \frac{\pi}{2} & m = n \end{cases}$$

Equation (13) can therefore be expressed as

$$I = \begin{cases} a\pi \tan \theta J_n(P_{ni}) J_n(P_{nj}) \left[\left(\frac{x}{P_{ni}} \right)^2 - \frac{n}{P_{ni}^2} - 1 \right] & m = n \\ 0 & m \neq n \end{cases} \quad (15)$$

A similar expression, differing only in subscripts, is obtained for the other line integral.

The necessary calculations having been performed, it is now possible to write the closed form solution for the coupling coefficient from one TE mode to another. Letting ψ_{ni} represent the original (p^{th}) mode, and ψ_{mj} the mode into which power is coupled, one obtains

$$S_{ip}^{\pm} = \frac{1}{2\sqrt{\beta_i \beta_p} (h_i^2 - h_p^2)} \left\{ \beta_i^2 h_p^2 \left[\left(\frac{n}{P_{nj}} \right)^2 - \frac{n}{P_{nj}^2} - 1 \right] \right. \\ \left. \pm \beta_p^2 h_i^2 \left[\left(\frac{n}{P_{ni}} \right)^2 - \frac{n}{P_{ni}^2} - 1 \right] \right\} a\pi \tan \theta J_n(P_{ni}) J_n(P_{nj}) \quad (16)$$

The same methodology can be used to derive the coupling coefficient from TE to TM modes. Defining the TM wave function to be

$$\psi_{mj} = J_m \left(\frac{q_{mj} a}{\rho} \right) \cos m \mp e^{-j k_z z} \quad (17)$$

it can be shown that

$$\begin{aligned}\frac{\partial \psi_{mj}}{\partial \rho} &= \cos m \phi e^{-j k_z z} \frac{\partial}{\partial \rho} J_m \left(\frac{q_{mj} a}{\rho} \right) \\ &= f(\rho) \cos m \phi e^{-j k_z z}\end{aligned}\quad (18)$$

and

$$\frac{\partial \psi_{ni}}{\partial s} = \frac{1}{\rho} \frac{\partial \psi_{ni}}{\partial \phi} = -\frac{n}{\rho} J_n \left(\frac{p_{ni} a}{\rho} \right) \sin n \phi e^{-j k_z z} \quad (19)$$

When equations (18) and (19) are introduced into the formula for the coupling coefficient, one obtains an equation of the form

$$S_{ip}^{\pm} \propto cf(\rho) \int_0^{2\pi} \cos m \phi \sin n \phi d\phi = 0 \quad (20)$$

There remains only to define an expression for the backward self coupling term S_{ii}^- . Again, following Solyar's equations, this term involves the evaluation of

$$I = \oint_C \tan \theta \left(\frac{\partial \psi}{\partial s} \right)^2 ds \quad (21)$$

Equation (19) has provided an expression for $\partial \psi / \partial s$, and noting that $ds = \rho d\phi$ one can write

$$\begin{aligned}I &= \int_0^{2\pi} \tan \theta \rho \left(-\frac{n}{\rho} \right)^2 J_n^2 \left(\frac{p_{ni} a}{\rho} \right) \Big|_{\rho=a} \sin^2 n \phi d\phi \\ &= \pi \tan \theta \frac{n^2}{a} J_n^2(p_{ni})\end{aligned}\quad (22)$$

which allows S_{ii}^- to be written as

$$S_{11}^- = -\pi/2 \tan \theta \frac{n^2}{a} J_n^2 (P_{n1}) \quad (23)$$

By drawing upon the above relationships (5) and (6), it is possible to obtain the amplitude of the spurious modes caused by changes in geometry of the tube. It is possible at this point to make a few generalized observations about this set of modified telegraphist's equations:

1. There will be no coupling between modes in a waveguide with constant radius ($\tan \theta = d \ln K / dz = 0$)
2. If the waveguide is axisymmetric, no energy is coupled between TE and TM modes. However, should the conductor be physically perturbed, coupling will occur.
3. These equations are valid for any slowly tapering waveguide. For this paper, only a linear taper was considered, but more complex geometries can be handled.
4. In order for coupling between TE modes to occur, the azimuthal mode numbers of the two modes must be the same.

A schematic representation of mode conversion is provided in Figure 4.

B. WINDOW CHARACTERISTICS

Before an optimization procedure can be devised, it is first necessary to accurately define the RF characteristics of a ceramic window. In order to arrive at such a definition, the window geometry must be

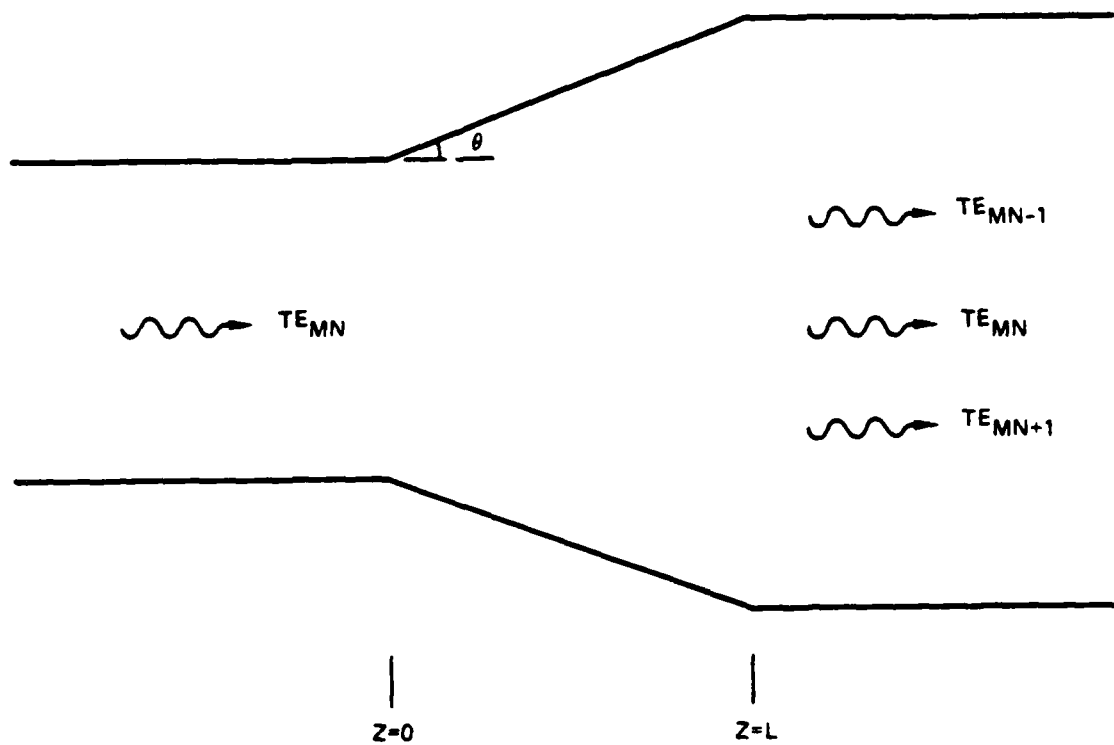


Figure 4 Mode conversion.

considered. Figure 5 shows a representation of a non-undercut five disc window of constant diameter. Three different dielectrics are used in this window, and the left face is exposed to vacuum while the right is exposed to air.

In order to analyze this window design, it was decided to use the two port transmission matrix approach as developed in Ramo². In this method, it is required that each of the planes indicated in Figure 5 be treated as a two port network. This multiplicity of planes, upon closer examination, resolves itself into two basic types of plane - an interface between dielectrics and a length of connecting waveguide (irregardless of whether air or dielectric filled).

It is perhaps easiest to begin by defining the transmission (T) matrix for a connecting waveguide section. It is obvious that this will consist of a phase shift between the forward and backward ports, or

$$T = \begin{bmatrix} e^{-j\beta l} & 0 \\ 0 & e^{j\beta l} \end{bmatrix} = \begin{bmatrix} \cos \beta l - j \sin \beta l & 0 \\ 0 & \cos \beta l + j \sin \beta l \end{bmatrix} \quad (24)$$

These matrices are used at planes b, d, f, h, and j.

The remaining planes constitute dielectric interfaces, and here the transmission matrix must be obtained through the application of boundary

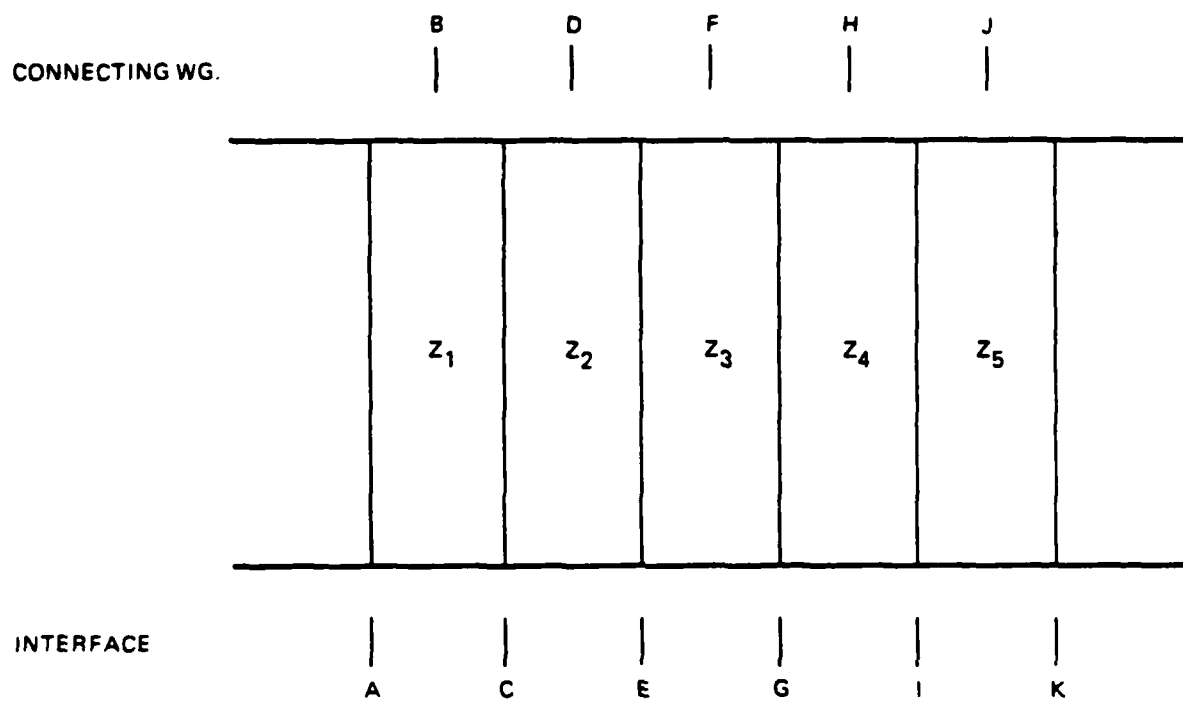


Figure 5 Window geometry.

conditions. It is known that across a dielectric boundary, the tangential components of the electric and magnetic fields are continuous. Referring to Figure 6, this can be expressed in terms of the incident and reflected wave amplitudes as

$$a_1 + b_1 = a_2 + b_2 \quad (25a)$$

$$\frac{1}{Z_1} (a_1 - b_1) = -\frac{1}{Z_2} (a_2 - b_2) \quad (25b)$$

Rearranging, one obtains

$$a_2 = a_1 \left(\frac{1 - Z_2/Z_1}{2} \right) + b_1 \left(\frac{1 + Z_2/Z_1}{2} \right) \quad (26a)$$

$$b_2 = a_1 \left(\frac{1 + Z_2/Z_1}{2} \right) + b_1 \left(\frac{1 - Z_2/Z_1}{2} \right) \quad (26b)$$

Or, expressing (26) in matrix form

$$T = \frac{1}{2} \begin{bmatrix} 1 + Z_2/Z_1 & 1 - Z_2/Z_1 \\ 1 - Z_2/Z_1 & 1 + Z_2/Z_1 \end{bmatrix} \quad (27)$$

The final transmission matrix for the system is the product of the individual matrices, or

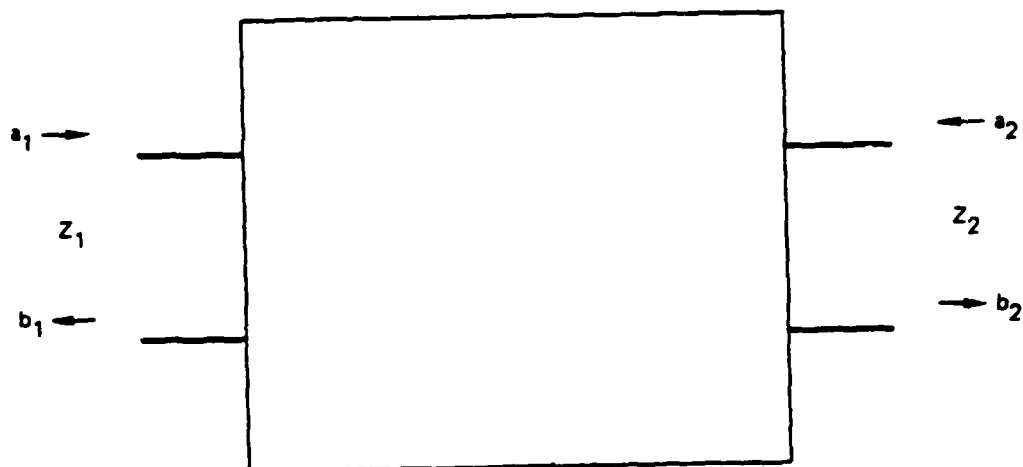


Figure 6 Two port network.

$$T = \prod_{i=1}^m T_i \quad (28)$$

A convenient parameter for expressing the efficiency of a window is its voltage standing wave ratio (VSWR), the ratio of the minimum and maximum values of the standing wave. The VSWR is defined as

$$VSWR = \frac{1 + |\rho|}{1 - |\rho|} \quad (29)$$

where ρ is the reflection coefficient of the system. Returning again to the two port representation, it can be seen that ρ , being the ratio of the reflected to the incident wave, is equal to b_1/a_1 when $a_2 = 0$.

Therefore

$$\rho = b_1/a_1 = -T_{21}/T_{22} \quad (30)$$

Introducing (30) into (29), one obtains

$$VSWR = \frac{1 + T_{21}/T_{22}}{1 - T_{21}/T_{22}} \quad (31)$$

Equation (31) is the form of the figure of merit that will be used in the subsequent computer program for window analysis. It should be noted that the transmission matrix elements used are complex and frequency dependent, leading to a finite bandwidth for low VSWR transmission.

An additional parameter of interest to window designers is that of power loss into the dielectric. The loss can be accurately represented by

$$P_{\text{loss}} = P_{\text{in}} (1 - e^{-2\alpha l}) \quad (32)$$

where the attenuation constant α is given by

$$\alpha = \frac{k}{2} \frac{\epsilon''}{\epsilon' \sqrt{1 - (f_c/f)^2}} \quad (33)$$

By using the series expansion $e^x = 1 + x$, (32) becomes

$$P_{\text{loss}} = 2\alpha l P_{\text{in}} \quad (34)$$

This expression will be used in Part III to help define the constraints on window optimization.

All of the calculations needed to define the problem of mode conversion and window analysis have been performed. It is now possible to proceed with the description of the numerical solutions and optimization technique.

III. NUMERICAL FORMULATION AND OPTIMIZATION

A. SOLUTION OF THE MODE CONVERSION EQUATIONS

In examining the coupled differential equations (5,6) for coupled mode amplitude, it must be remembered that in order to allow a numerical solution to be found, the boundary conditions must be defined. Solymar has stated that the boundaries are as follows:

$$A_m^+(0) = A_0 \quad A_i^+(0) = 0 \quad A_m^-(L) = 0 \quad A_i^-(L) = 0 \quad (35)$$

where the subscript m denotes the original (driving) mode and i the coupled spurious modes. These conditions can be interpreted as meaning that the system is fed by only one mode and that no modes are being introduced back into the output.

Upon first glance, it would appear that the ordinary differential equations plus boundary conditions combine to yield a straightforward coupled initial value problem. A closer inspection reveals that whereas the initial conditions for the forward modes are given at $z = 0$, those for the backward modes are given at $z = L$. It would appear then that the standard methods of solution for initial value problems (Runge-Kutta, predictor-corrector, etc.) are inapplicable, and that the system of equations must be modified to allow solution through the use of a two point boundary value technique, such as shooting. One would like to avoid such a modification, as it greatly complicates the problem, requiring solution of a higher order system and increasing computing time.

However, an alternative is available. Saad³ has indicated that a technique developed by Derman⁴, known as invariant imbedding, has proved applicable to this problem. Since the full force of the imbedding technique was not required for the problem at hand, a full discussion of the invariant imbedding method will not be undertaken here; those interested should consult Derman.

In order to apply the invariant technique, one must be able to consider the set of equations

$$\frac{d u(z)}{dz} = a(z) u(z) + b(z) v(z) + e(z) \quad (36a)$$

$$- \frac{d v(z)}{dz} = c(z) u(z) + d(z) v(z) + f(z) \quad (36b)$$

$$u(0) = u_0 \quad v(1) = 0 \quad (36c)$$

Inspection of Solyman's equations (5,6) reveals that they are of this form, if the following substitutions are made:

$$\begin{aligned} u(z) &= A_1^+(z) & v(z) &= A_1^-(z) \\ a(z) &= -j \beta_1 = d(z) & b(z) &= -\frac{1}{2} \frac{d \ln K_1}{dz} = -c(z) \\ e(z) &= \sum_p \left(S_{1p}^+ A_p^+ + S_{1p}^- A_p^- \right) & f(z) &= \sum_p \left(S_{1p}^- A_p^+ + S_{1p}^+ A_p^- \right) \end{aligned} \quad (37)$$

With this change of variables, the solution may proceed. As equations (36a) and (36b) are similar, a solution will be presented in detail only for (36a).

To begin with, it is required that the variable $u(z)$ be replaced through the use of a modified Ricatti transformation:

$$u(z) = r_1(z) v(z) + r_2(z) \quad (38)$$

where $r_1(z)$ and $r_2(z)$ are unknown functions whose form will be found presently. Differentiating (38) with respect to z yields

$$\frac{du}{dz} = r_1 \frac{dv}{dz} + r_1' v + r_2' \quad (39)$$

Substituting (36a) and (36b) into (39)

$$au + bv + e = r_1(-cu - dv - f) + r_1'v + r_2' \quad (40)$$

(Each term in the above equation is a function of z ; indication of dependency has been dropped in the interest of clarity.)

Making use of (38) in (40)

$$a(r_1v + r_2) + bv + e = r_1[-c(r_1v + r_2) - dv - f] + r_1'v + r_2'$$

Collecting terms

$$v[(a + d)r_1 + b + cr_1^2 - r_1'] + [(a + cr_1)r_2 + fr_1 + e - r_2'] = 0$$

Finally, setting the terms in brackets to zero

$$r_1' = b + (a + d)r_1 + cr_1^2 \quad (41a)$$

$$r_2' = (a + cr_1)r_2 + fr_1 + e \quad (41b)$$

Considering the point $z = 0$, it can be seen that (38) becomes

$$u(0) = r_1(0)v(0) + r_2(0)$$

Letting $r_1(0) = 0$ (as it is an arbitrary function its initial value may also be arbitrarily chosen), it becomes apparent that $u(0) = r_2(0) = u_0$.

Similarly, if one lets $v(0) = q_1(z)v(z) + q_2(z)$, one obtains

$$q_1' = (d + cr_1)q_1 \quad (42a)$$

$$q_2' = (f + cr_2)q_1 \quad (42b)$$

with $q_1(0) = 1$ and $q_2(0) = 0$. Therefore

$$v(0) = q_1(l)v(l) + q_2(l) \quad (43)$$

and

$$v(z) = \frac{v(0) - q_2(z)}{q_1(z)} = \frac{q_1(l)}{q_1(z)} v(0) + \frac{q_2(l) - q_2(z)}{q_1(z)} \quad (44)$$

Pausing now to look back over the preceeding equations, it can be seen that the original system of equations (36a,b) has been replaced by a set of four differential equations, (41a,b) and (42a,b), which along with their boundary conditions form a coupled initial value problem. The four quantities (r_1 , r_2 , q_1 , q_2) can be related back to the original u and v through the use of (38) and (44). The relationship between these newly defined variables and the quantities expressed in Solymar's equations is diagrammed in Figure 7.

It remains, however, to obtain an explicit numerical solution to this set of differential equations. To do so, it was decided to use a multistep technique, such as a predictor-corrector, rather than a single-step method like Runge-Kutta. This choice was based on the fact that single-step methods use the values obtained at only the previous step in order to calculate the function value at the subsequent step, whereas multistep techniques make use of the data obtained at several previous points to calculate the next step. Thus the multistep method is better equipped to track a quickly varying function, as it would be less likely to incorrectly predict the next function value.

The predictor-corrector method carries a further advantage in that it utilizes both implicit and explicit forms to obtain a solution. An implicit form is one where the value of a dependent variable at a subsequent step is defined in terms of itself, i.e., $y_{n+1} = f(x_{n+1}, y_{n+1})$. However, since one is usually interested in determining y_{n+1} , this method cannot be directly applied. Initially, therefore, it is necessary to

$$\dot{r}_1 = \frac{1}{2} \frac{d \ln K_i}{dz} r_1^2 - \frac{1}{2} \frac{d \ln K_i}{dz} - j 2 \beta_i r_1$$

$$\begin{aligned} \dot{r}_2 = & \left(-j \beta_i + \frac{1}{2} \frac{d \ln K_i}{dz} r_1 \right) r_2 + \sum_p \left(S_{ip}^+ A_p^- + S_{ip}^- A_p^+ \right) r_1 \\ & + \sum_p \left(S_{ip}^+ A_p^+ + S_{ip}^- A_p^- \right) \end{aligned}$$

$$\dot{q}_1 = \left(-j \beta_i + \frac{1}{2} \frac{d \ln K_i}{dz} r_1 \right) q_1$$

$$\dot{q}_2 = \left[\sum_p \left(S_{ip}^+ A_p^- + S_{ip}^- A_p^+ \right) + \frac{1}{2} \frac{d \ln K_i}{dz} r_2 \right] q_1$$

$$q_1(0) = 1$$

$$q_2(0) = 0$$

$$r_1(0) = 0$$

$$r_2(0) = A_0$$

Figure 7 Riccatti transforms of Solymar's equations.

employ the explicit form of the solution, one where the subsequent step is defined by the previous step, or $y_{n+1} = f(x_{n+1}, y_n)$.

The Adams-Moulton predictor-corrector used to solve the problem of interest uses an explicit method as the predictor and an implicit method (using y_{n+1} obtained from the predictor) to correct the approximated solution. Since Adams-Moulton is a fourth order method, it calculates the new function value from the three previous values. In order to obtain these initial points, Runge-Kutta was applied for the first three steps, whereupon the Adams-Moulton form was used:

Predictor

$$y_4^{(0)} = y_3 + \frac{h}{24} \left[55 f(x_3, y_3) - 59 f(x_2, y_2) + 37 f(x_1, y_1) - 9 f(x_0, y_0) \right] \quad (45a)$$

Corrector

$$y_4^{(1)} = y_3 + \frac{h}{24} \left[9 f(x_4, y_4^{(0)}) + 19 f(x_3, y_3) - 5 f(x_2, y_2) + f(x_1, y_1) \right] \quad (45b)$$

This method was applied to the system of equations shown in Figure 7 in order to obtain r_1 , r_2 , q_1 , and q_2 at each interval in the taper region. Once these values have been found, it is a simple matter to obtain the magnitudes of the forward and backward waves for each mode throughout the taper.

The analysis described above was performed on both the uptaper and downtaper regions shown in Figure 1. Since the coupling coefficients are equal to zero in regions where the waveguide diameter is unchanging, there was no need to perform calculations through the actual collector

region itself. The final amplitudes from the uptaper were used as the starting conditions for the downtaper.

As was mentioned before, only a linear taper was considered during the problem solution. However, the only modification needed to be performed to the above routine in order to permit the handling of more complex geometries is the addition of a short "preprocessor" program to supply the radius and $\tan \theta$ values at each iterative step. Also, since this project dealt with window design, only the mode content at the window was considered important. However, this method will allow for the solution for the mode content at any point in the collector region, as well as the calculation of the voltage travelling wave ratio (VTWR) as defined by Stone⁵:

$$VTWR = \pm \frac{|A_n| + |A_m|}{|A_n| - |A_m|} \quad (46)$$

where A_n and A_m are the amplitudes of two modes. This VTWR is a measurable quantity representing the beat pattern resulting from the superposition of two traveling waves. This physical parameter allows for the possible experimental verification of the mode content.

By using a predictor-corrector on the Ricatti transformation of Solymer's modified telegraphist's equations, it has become possible to characterize the mode content of the RF energy incident upon the window, and can now proceed to the actual optimization of the window thickness.

B. OPTIMIZATION OF WINDOW THICKNESS

When designing a window, it is desirable to have the lowest possible VSWR over the widest possible bandwidth. One implementation of this transmission profile is the Butterworth or maximally flat response, where the VSWR increases smoothly from unity in either direction from the center frequency. This response function is desirable in that minor variations in frequency will not cause an abrupt change in transmission, as can occur with other filter (window) responses.

Achieving such a transmission characteristic has until now implied searching for the combination of window thicknesses (assuming known diameters and dielectric constants) by either the laborious process of cold testing various combinations or repeating the calculation of the window characteristic with varying widths; at best, a tedious procedure. Whereas at lower frequencies a lumped element analysis or quarter wavelength method can be used, these both assume that the impedance of the window can be varied to exactly match the calculated value. At gyrotron frequencies, only a few window materials are available, and for ease of construction it is desirable to obtain a constant window diameter, so the low frequency techniques are inapplicable.

It is therefore necessary to determine another method of optimization. Optimization by itself implies a search for the best condition, so in effect the problem involves seeking a combination of window thicknesses. To do so, a technique known as the simplex method was applied.

The simplex method, as developed by Nelder and Mead⁷, is a means of searching for either maxima or minima. A simplex is an area in n -space defined by $n+1$ vertices which are linearly independent and all line segments connecting them. The vertices consist of the function values evaluated at $n+1$ randomly defined points in n -space (Figure 8). This rather odd appearing construct locates a minimum in the following fashion: first, the point associated with the highest function value P_H is identified. This point is replaced by a new point defined as the reflection of f_H through the centroid \bar{P} (the center of all points other than f_H) according to

$$P^* = (1 + \alpha) \bar{P} - \alpha P_H \quad \alpha \leq 1 \quad (47)$$

The function value at the new point P^* is now found. Should it prove to be the lowest function value, a further expansion in that direction is performed by

$$P^{**} = \gamma P^* + (1 - \gamma) \bar{P} \quad \gamma > 1 \quad (48)$$

If $f(P^{**}) < f_L$, then P_H is replaced by P^{**} ; otherwise, it is replaced by P^* .

Occasionally, though, it will occur that the reflected point P^* is associated with a function value which is still greater than that at any other point, i.e., $f(P^*) = f_H$. At this point it becomes necessary to contract the point $\min(P_H, P^*)$ back toward the centroid using

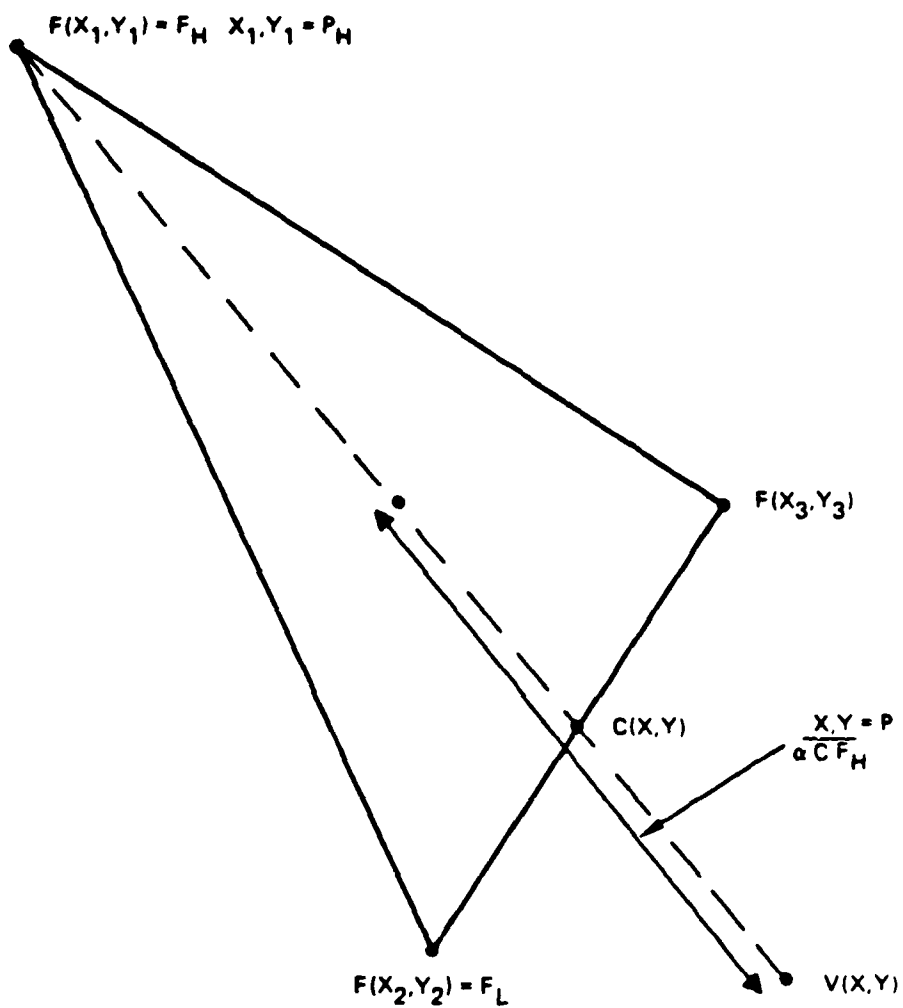


Figure 8 Two dimensional simplex.

$$P^{**} = \beta P_H + (1 - \beta) \bar{P} \quad 0 < \beta < 1 \quad (49)$$

If the problem persists, that is $f(P^{**}) > f_H$, it is an indication that a minimizing value is located within the bounds of the simplex, so the entire simplex (not just P_H) is contracted by replacing all points (P_i) by $1/2(P_i + P_L)$. This shrinking of the area will continue until the minimum is found or is placed outside of the simplex.

A simplex can be envisioned as following the topology steadily downward, its speed of descent in direct proportion to the gradient; the steeper the slope, the faster the simplex proceeds. Upon reaching a valley containing a minimum, it contracts about it until the stopping conditions for the search are met. The simplex method does however have one major flaw. It is unable to distinguish between a local and a global minimum (Figure 9). Once it enters a valley, it will proceed to the lowest point in the valley, regardless of whether a neighboring valley contains an even lower function value. This problem will be addressed as the solution develops.

Before beginning the search itself, it proves efficacious to define the area to be searched a bit more closely. The VSWR, which is the function to be minimized, is dependent upon the thicknesses of the n windows and the frequency, or $n+1$ variables altogether. A little thought reveals that searching all $n+1$ variables would involve looking for the exact VSWR vs frequency response desired. This is a favorable goal, but hardly a practical one. Should the actual available response differ even

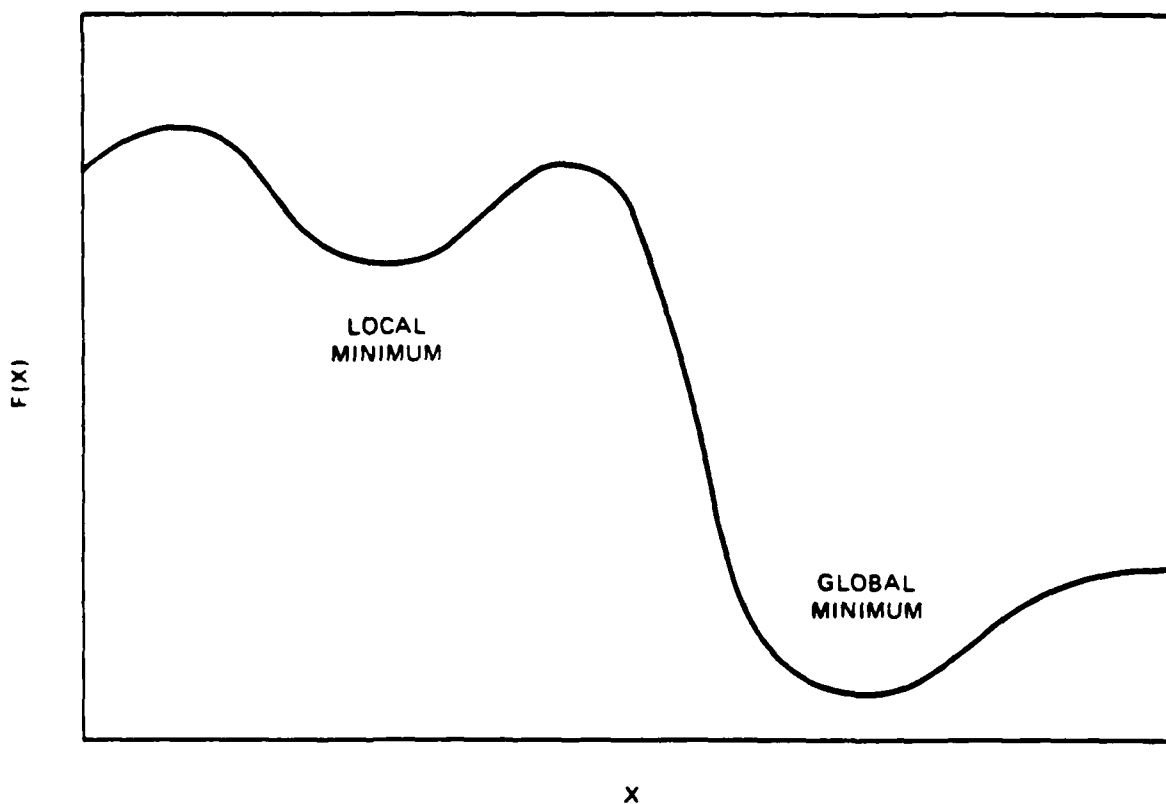


Figure 9 Global and local minima.

slightly from the ideal values, the search will fail. Additionally, the simplex technique by itself performs on the order of n calculations at each step, while the evaluation of the function (as per Section II.A) employs $O(n^2)$ operations; thus it would be beneficial to reduce n .

The scheme used herein avoids both these problems. Since it is known that the lowest VSWR should occur at the center of the band, the search used in this project held its frequency variable fixed at the center frequency, eliminating that variable. Once the center band minimum had been found, the response over the bandwidth would be examined.

Up until now, no mention had been made of exactly what area is to be searched. The search parameters have been narrowed down to only the window thicknesses, but searching for every possible width combination would prove temporally impossible as well as yielding impractical results (such as the trivial solution). Two limiting factors do however exist. The first is associated with the fact that the window must bear the mechanical stress of maintaining a vacuum, so that it must be thick enough that it will not be collapsed by the pressure difference. At the same time, it will be remembered that the power absorbed by a window is directly related to its thickness (Eq. 34), so that an overly wide window would absorb a large amount of RF energy, introducing thermal stress which can lead to cracking and window failure. These two mechanical considerations therefore define the upper and lower parameters for each of the search variables. In practice, they can be determined either by a detailed mechanical analysis relating maximum permissible power loss

and stress strength to thickness, or, as appears to be more commonly done, by intuitive approximation.

Now that the search region has been constrained, one further obstacle remains to be removed. It was mentioned earlier that the simplex can become trapped in a local minimum without locating a global minimum. This problem was circumvented by dividing the region into smaller areas, thus lowering the chances that one area would contain more than one minimum. A simplex was released into each subdivision; if no minimum was found after a predetermined number of iterations, the method proceeded to another subdivision. If a minimum was found, the coordinates of the point (window lengths) were stored and searching was contained in another region. The stopping criterion used was that the function value should be a small difference away from the minimum value (which, for VSWR, is 1) or

$$\text{VSWR} - 1 \leq \epsilon \quad (50)$$

After every subregion has been examined, each discovered minimum is subjected to the following inspection to determine if it meets the transmission requirements. The value of the VSWR is calculated at eight additional points - center frequency (f_c) + bandwidth/2 ($BW/2$), $f_c - BW/2$, $f_c + BW/4$, $f_c - BW/4$, $f_c + BW/2 + \epsilon$, $f_c - BW/2 + \epsilon$, $f_c + BW/4 + \epsilon$, $f_c - BW/4 + \epsilon$, where ϵ is a small frequency spacing unrelated to the ϵ in Eq. 50. The reason for calculating the function value at pairs of closely spaced points is to enable calculation of the derivative of the function

at these points. If the function values are within the specified limits for VSWR across the band, and the derivative indicate no wild oscillations, the combination of thicknesses is declared to be a viable one. Occasionally, more than one combination will be passed, whereupon it falls to the user to select the more desirable of the two, whether by transmission, machining ease, or lower overall power absorption.

IV. CALCULATED RESULTS

It is always expedient (as well as reassuring) to be able to verify that a theory coincides with actuality, though it is not always easy to do so. It was not within the scope of this project to experimentally verify the accuracy of the developed design technique, so in order to prove its validity the methods proposed in this paper were applied to already known situations.

To confirm the mode coupling solution, the results presented by the program were compared against those obtained by a similar method by Stone.⁵ Having access to greater resources, Stone was able to experimentally determine that the calculations matched reality to $\pm 5\%$. Therefore, agreement with Stone's results would vindicate the method proposed in this paper. As can be seen in Figure 10, close agreement was obtained. The differences that occur are most plausibly explained by the fact that the two methods used different routines to solve the differential equations.

Window optimization was validated by an attempt to recreate the values currently in use at Hughes Aircraft Company. The three frequencies chosen (28, 60 and 100 GHz) represent existing gyrotrons whose window transmission characteristics are considered acceptable. Shown in Figures 11 to 16 are the parameters used in the calculations, the computer generated results, and the actual design dimensions. Discrepancies in these results, though slight, are the result of machining considerations -

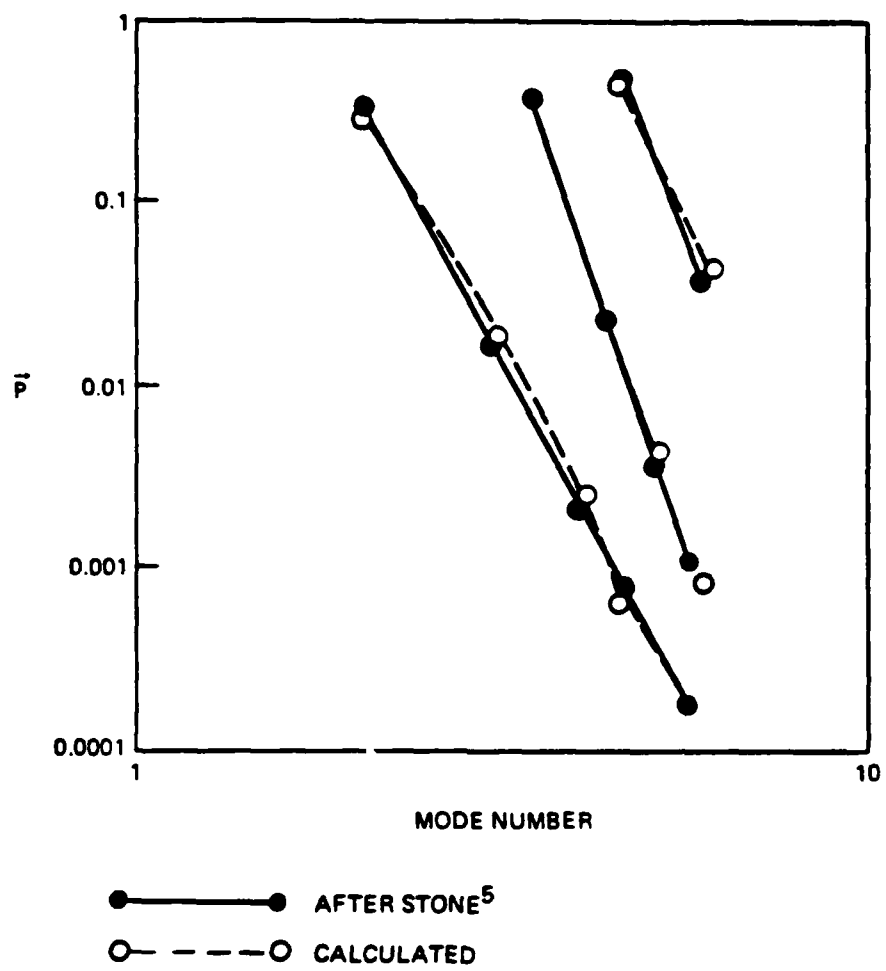


Figure 10 Mode content.

A. DESIGN PARAMETERS

CENTER FREQUENCY	28 GHz
PEAK POWER	100 kW
BANDWIDTH	4 GHz BELOW VSWR = 1.75
MODE,	TE _{o2} ($\rho_{ni} = 7.0155$)
NO. OF WINDOW ELEMENTS	3
DIELECTRIC CONSTANTS	3.8, 9.6, 3.8
LOSS TANGENTS	0.00158, 0.00068, 0.00158
WINDOW DIAMETER	3 in.
MAX. POWER LOST IN EACH WINDOW ELEMENT	0.5, 0.5, 0.5 kW
MAXIMUM SLOPE $\left(\frac{d \text{ VSWR}}{df}\right)$	0.35
MAXIMUM VSWR AT CENTER FREQUENCY	1.05

B. OPTIMIZED WINDOW

WINDOW THICKNESS (W)	0.055, 0.0675, 0.055
POWER LOST IN EACH SECTION	0.13, 0.069, 0.13 kW

Figure 11 28 GHz window parameters.

HUGHES MULTI DISC WINDOW DESIGN

DISC WIDTH = 0.0000
WAVELENGTHS - 0.0000

CERAM. WIDTH = 0.0550
WAVELENGTHS - 0.2510

CEN SPACING = 0.0675
WAVELENGTH - 0.4936

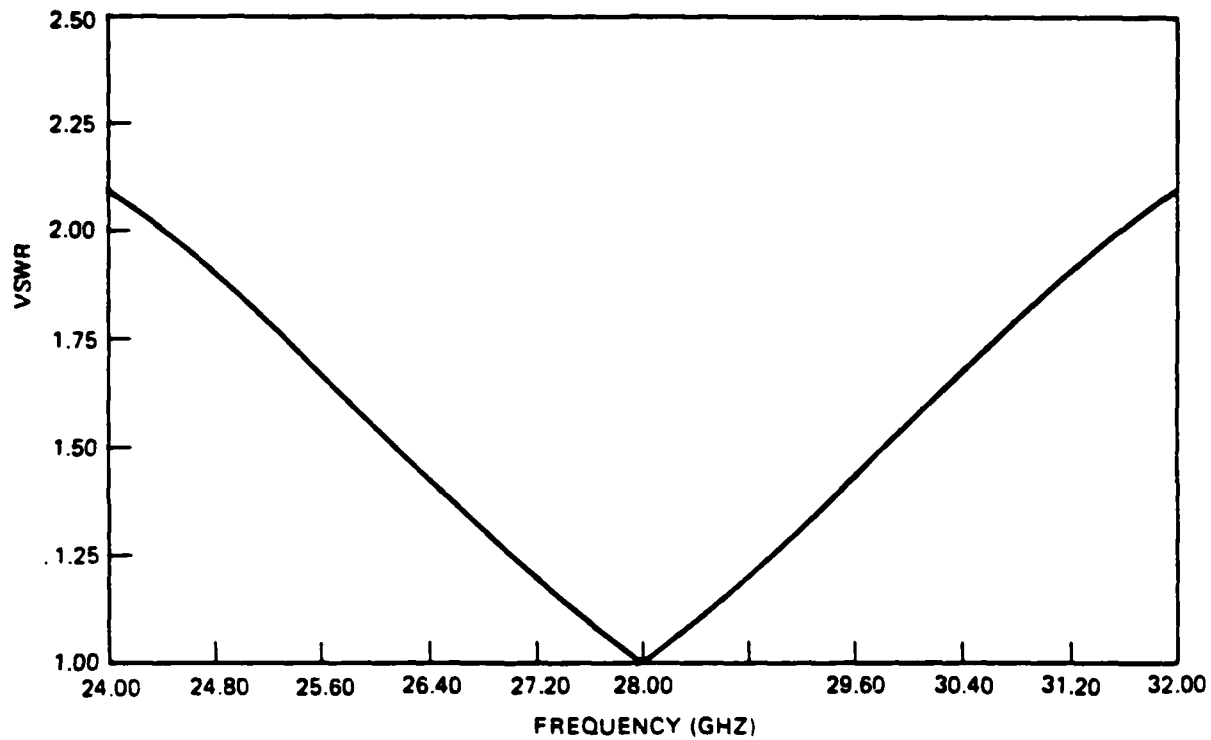


Figure 12 28 GHz window response.

A. DESIGN PARAMETERS

CENTER FREQUENCY	60 GHz
PEAK POWER	200 kW
BANDWIDTH	3 GHz BELOW VSWR = 1.5
MODE	TE ₀₂ ($p_{ni} = 7.0155$)
NO. OF WINDOW ELEMENTS	5
DIELECTRIC CONSTANTS	3.8, 9.6, 1.75, 9.6, 3.8
LOSS TANGENTS	0.00158, 0.00068, 0.005, 0.00068, 0.00158
WINDOW DIAMETER	2 in.
MAX. POWER LOST IN EACH WINDOW ELEMENT	1, 1, 3, 1, 1 kW
MAXIMUM SLOPE $\left(\frac{d \text{ VSWR}}{df}\right)$	0.4
MAXIMUM VSWR AT CENTER FREQUENCY	1.1

B. OPTIMIZED WINDOW

WINDOW THICKNESS (IN)	0.073, 0.088, 0.0805, 0.088, 0.073
POWER LOST IN EACH SECTION	0.74, 0.39, 2.58, 0.39, 0.74 kW

Figure 13 60 GHz window parameters.

HUGHES MULTI DISC WINDOW DESIGN

DISC WIDTH = 0.0730
WAVELENGTHS - 0.7188

CERAM. WIDTH = 0.0880
WAVELENGTHS - 1.3827

CEN SPACING = 0.0805
WAVELENGTHS - 0.5339

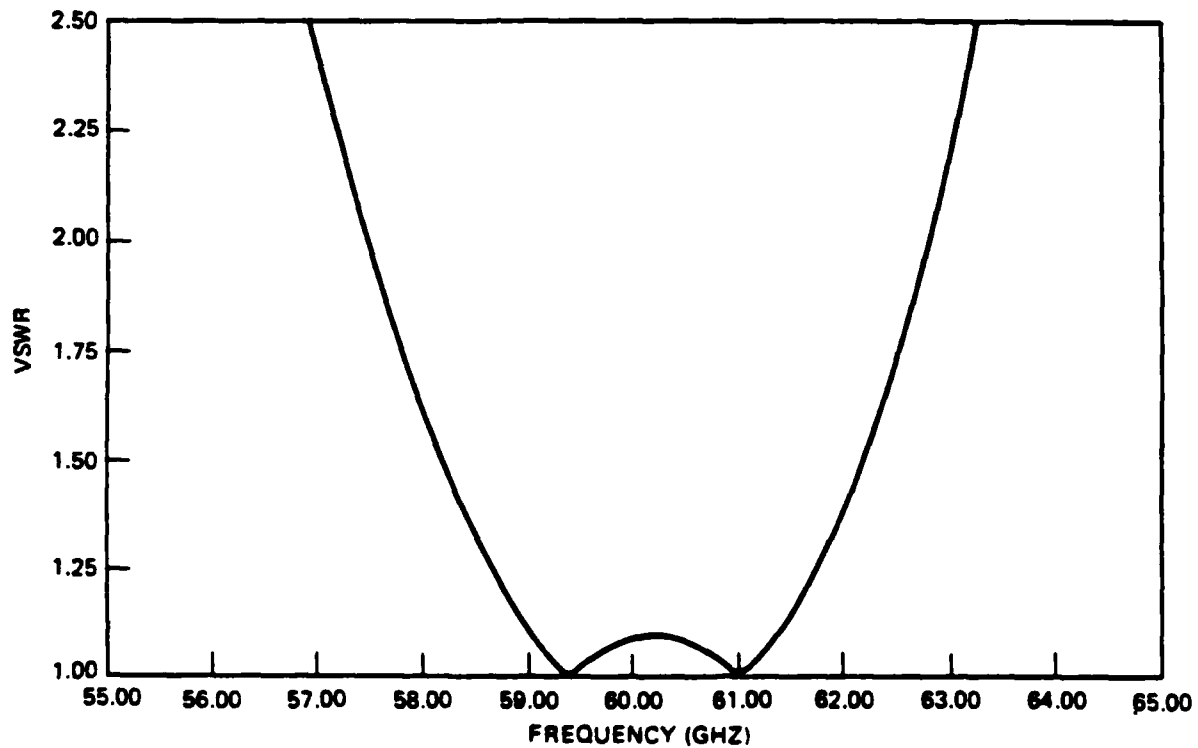


Figure 14 60 GHz window response.

A. DESIGN PARAMETERS

CENTER FREQUENCY	100 GHz
PEAK POWER	500 kW
BANDWIDTH	5 GHz BELOW VSWR = 1.5
MODE	TE ₀₄ ($p_{ni} = 13.324$)
NO. OF WINDOW ELEMENTS	5
DIELECTRIC CONSTANTS	3.8, 9.6, 1.75, 9.6, 3.8
LOSS TANGENTS	0.00158, 0.00068, 0.005 0.00068, 0.00158
WINDOW DIAMETER	2 in.
MAX. POWER LOST IN EACH WINDOW ELEMENT	2, 2, 8, 2, 2 kw
MAXIMUM SLOPE $\left(\frac{d \text{ VSWR}}{df}\right)$	0.4
MAXIMUM VSWR AT CENTER FREQUENCY	1.05

B. OPTIMIZED WINDOW

WINDOW THICKNESS (IN.)	0.045, 0.052, 0.049, 0.052, 0.045
POWER LOST IN EACH SECTION	1.90, 0.952, 6.52, 0.952, 1.90 kW

Figure 15 100 GHz window parameters.

HUGHES MULTI DISC WINDOW DESIGN

DISC WIDTH = 0.0450
WAVELENGTHS - 0.7371

CERAM. WIDTH = 0.0520
WAVELENGTHS - 1.3607

CEN SPACING = 0.0490
WAVELENGTHS - 0.5393

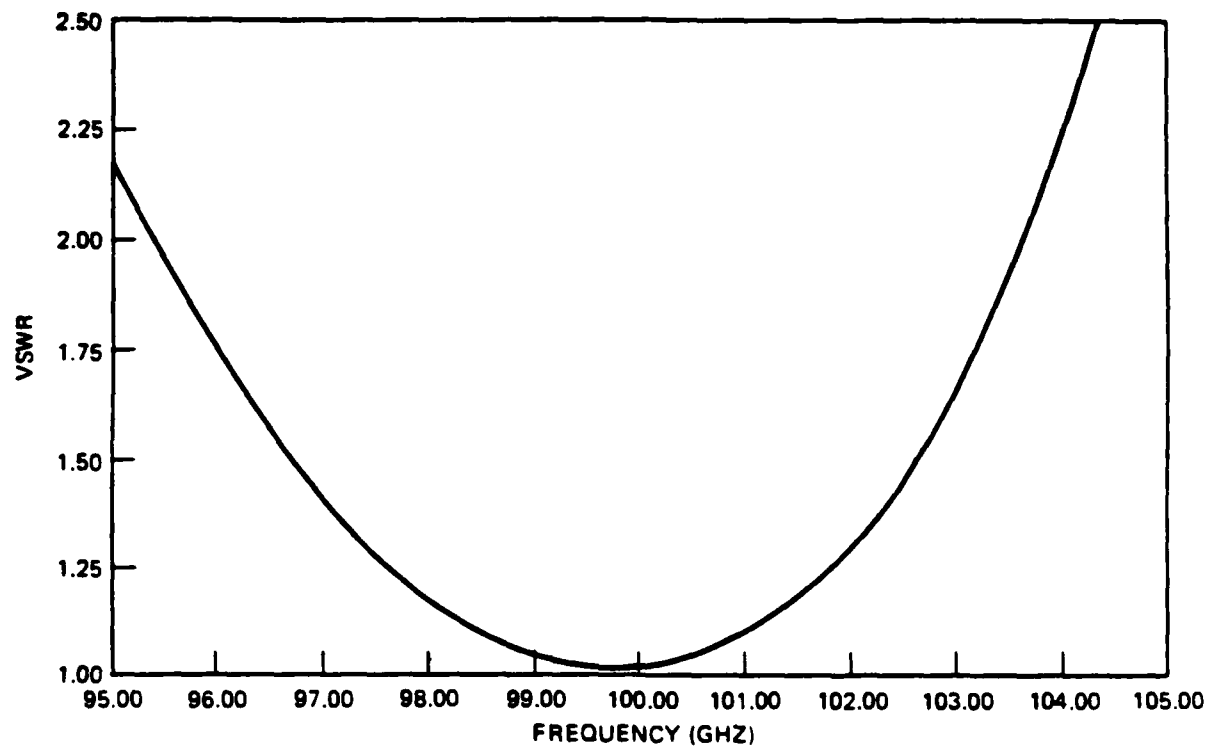


Figure 16 100 GHz window response.

it is impractical to specify dimensions to tenths of mils. An additional note - it was experimentally determined that slight differences in window diameter do not affect the VSWR as strongly as predicted by computer calculations.

The optimization program, being written as part of a research project, is slightly esoteric in its operation and requires a slight degree of finesse in choosing the starting conditions. It was found that four factors are primarily responsible for those numerous occasions during program development when no answers were returned. First, if the limits imposed upon the lengths are too close, there may not be a minimum contained in the region. This can occur if one attempts to specify an upper limit (thermal limit) too close to the mechanical limit, i.e., constrain the problem severely toward the thinnest possible window. Another problem arising from the user asking for too much comes from requiring that the VSWR must be close to one across the entire band. This simply cannot always be achieved.

The above errors are caused by requiring the program to produce an impossibly ideal design. Two further factors enter as a result of the method itself. Should the subregions be made too large, the simplex may trap itself in a local minimum and be unable to locate an optimum solution. Similarly, should the function be extremely smooth, the simplex, whose rate of descent is determined by the slope of the function, may not be able to converge to a solution within the maximum number of stages. These two problems can only be avoided by developing an intuitive feel

for what are convenient values for these parameters. Alternately, should termination occur due to these errors, the appropriate value can be altered and the program rerun.

V. CONCLUSIONS

As was shown in the proceeding section, agreement with actual results was good. Variations occurred either from different calculation techniques or alteration of results to meet physically realizable conditions. This similarity of results leads one to conclude that the methods presented in this paper can be used in the future as the principle method of window design.

Originally, it was intended to combine the mode content results with the window optimization routine, designing the window so as to allow transmission of more than one mode. Unfortunately, however, a creditable means of weighing the modes so as to assign priority in transmission characteristics proved unobtainable. This, along with allowing for curved window surfaces, are fertile ground for future work.

BIBLIOGRAPHY

1. Solyman, L. Spurious Mode Generation in Nonuniform Waveguide, IRE Transactions in Microwave Theory and Techniques, July 1959, pp. 379-383.
2. Ramo, S., Whinnery, J., Van Duzer, T. Fields and Waves in Communication Electronics. John Wiley 1965.
3. Saad S., Davies, J. Computer Analysis of Gradually Tapered Waveguide, IEEE MTT, May 1977, pp. 437-440.
4. Detman, E. Coupled Modes in Plasmas, Elastic Media, and Parametric Amplifiers. Elsevier, 1970.
5. Stone, D. Measurement of VSWR and Mode Content in Multimode Waveguides, presented Dec. 1, 1983, Univ. of Utah AFTER Program lecture.
6. Burden, R. Numerical Analysis, Prindle, Weber and Schmidt, 1981.
7. Nelder, J. and Mead, R. A Simplex Method for Function Minimization.

END

FILMED

6-86

DTIC